Multimodal MRI Can Identify Perfusion and Metabolic Changes in the Invasive Margin of Glioblastomas

Stephen J. Price, PhD FRCS (Neuro.Surg),[1,2]* Adam M.H. Young, MRCS,[1] William J. Scotton, MRCS,[1] Jared Ching, MB ChB,[1] Laila A. Mohsen, MD,[3] Natalie R. Boonzaier, MSc,[1,2] Victoria C. Lupson, BSc,[2] John R. Griffiths, DPhil FRCP,[4] Mary A. McLean, PhD,[4] and Timothy J. Larkin, PhD[1,2]

Purpose: To use perfusion and magnetic resonance (MR) spectroscopy to compare the diffusion tensor imaging (DTI)-defined invasive and noninvasive regions. Invasion of normal brain is a cardinal feature of glioblastomas (GBM) and a major cause of treatment failure. DTI can identify invasive regions.
Materials and Methods: In all, 50 GBM patients were imaged preoperatively at 3T with anatomic sequences, DTI, dynamic susceptibility perfusion MR (DSCI), and multivoxel spectroscopy. The DTI and DSCI data were coregistered to the spectroscopy data and regions of interest (ROIs) were made in the invasive (determined by DTI), noninvasive regions, and normal brain. Values of relative cerebral blood volume (rCBV), N-acetyl aspartate (NAA), myoinositol (mI), total choline (Cho), and glutamate + glutamine (Glx) normalized to creatine (Cr) and Cho/NAA were measured at each ROI.
Results: Invasive regions showed significant increases in rCBV, suggesting angiogenesis (invasive rCBV 1.64 [95% confidence interval, CI: 1.5–1.76] vs. noninvasive 1.14 [1.09–1.18]; $P < 0.001$), Cho/Cr (invasive 0.42 [0.38–0.46] vs. noninvasive 0.35 [0.31–0.38]; $P = 0.02$) and Cho/NAA (invasive 0.54 [0.41–0.68] vs. noninvasive 0.37 [0.29–0.45]; $P = < 0.03$), suggesting proliferation, and Glx/Cr (invasive 1.54 [1.27–1.82] vs. noninvasive 1.3 [1.13–1.47]; $P = 0.028$), suggesting glutamate release; and a significantly reduced NAA/Cr (invasive 0.95 [0.85–1.05] vs. noninvasive 1.19 [1.06–1.31]; $P = 0.008$). The mI/Cr was not different between the three ROIs (invasive 1.2 [0.99–1.41] vs. noninvasive 1.3 [1.14–1.46]; $P = 0.68$). In the noninvasive regions, the values were not different from normal brain.
Conclusion: Combining DTI to identify the invasive region with perfusion and spectroscopy, we can identify changes in invasive regions not seen in noninvasive regions.

J. MAGN. RESON. IMAGING 2016;43:487–494.

Despite our improved knowledge and understanding of glioblastomas (GBM), they still carry a dismal prognosis. Survival can be improved by more aggressive surgical resections[1] and the combination of radiotherapy and chemotherapy, yet virtually all patients will die from progressive disease. This disease progression is usually within the high dose area of radiotherapy[2–5] in an area of tumor invasion. This invasive margin is a cardinal feature of GBM and is one of the major causes of treatment failure.[6] As the invasive margin cannot be accurately identified with clinical, anatomical imaging (T_1-weighted,

View this article online at wileyonlinelibrary.com. DOI: 10.1002/jmri.24996

Received Feb 20, 2015, Accepted for publication Jun 23, 2015.

*Address reprint requests to: S.J.P., Neurosurgery Division, Department of Clinical Neurosciences, University of Cambridge, Box 167, Cambridge Biomedical Campus, Cambridge CB2 0QQ, UK. E-mail: sjp58@cam.ac.uk

The copyright line for this article was changed on 20 October 2015 after original online publication.

From the [1]Neurosurgery Division, Department of Clinical Neurosciences, University of Cambridge, Cambridge Biomedical Campus, Cambridge, UK; [2]Wolfson Brain Imaging Centre, Department of Clinical Neurosciences, University of Cambridge, Cambridge Biomedical Campus, Cambridge, UK; [3]University Department of Radiology, University of Cambridge, Cambridge Biomedical Campus, Cambridge, UK; and [4]Cancer Research UK Cambridge Institute, University of Cambridge, Li Ka Shing Centre, Cambridge, UK.

T_2-weighted, and fluid-attenuated inversion recovery [FLAIR] imaging),[7,8] new imaging methods are required to delineate it and to facilitate study of its biology.

Our understanding of what happens in the invasive margin is less well developed than for the center of the tumor. It is known that invading cells have a different phenotype and are more motile and less proliferative.[9] The release of enzymes (such as metalloproteases) breaks down the extracellular matrix and the release of glutamate (secondary to disruption of the glial matrix) destroys glia and neuronal processes to provide space for tumor cells to invade.[10,11] As cell numbers increase the tumor cells become hypoxic, providing an important trigger for changes both in brain metabolism and angiogenesis that will lead to further tumor cell invasion.[12] Invasion is therefore a multistage, multicellular process that cannot be completely studied using a single method.

As invasion primarily involves white matter tracts, imaging disruption of the architecture of the white matter will be vital in identifying tumor invasion. Diffusion tensor magnetic resonance imaging (DTI) is a technique sensitive to the ordered diffusion of water along white matter tracts, and it can detect subtle disruption. Studies have shown that it can identify changes in white matter on the periphery of an invasive GBM that are not seen in noninvasive metastases[13,14] or meningiomas,[15] suggesting that these changes in the peritumoral area are due to invasion. Diffusion tensor tissue signatures can split the tensor information into isotropic diffusion (p: magnitude of diffusion) and anisotropic diffusion (q: measure of the directionality of diffusion).[16] This procedure can differentiate regions of pure tumor (reduced q and increased p) from invaded white matter (increased p alone)[17] and is more sensitive than conventional DTI measures such as fractional anisotropy (FA).[8,18] Image-guided biopsies of these regions have confirmed invasive tumor with a high degree of accuracy in both high-grade gliomas[8] and low-grade gliomas.[19] Follow-up studies have shown that these regions predate the development of contrast enhancement at progression, and can predict the time to tumor progression[20] and its pattern.[21,22] This provides a valuable method of identifying the invasive tumor margin.

Dynamic susceptibility contrast perfusion imaging (DSCI) provides information on the relative cerebral blood volume (rCBV) that correlates with tumor vascularity[23,24] and cellular proliferation.[25] Multivoxel MR spectroscopy (MRS), or chemical shift imaging (CSI), reveals changes in tissue metabolism within the invasive region. In this study we aimed to understand the local environment of GBM by exploring the perfusion and metabolic changes seen in the DTI-defined invasive margin of GBMs and compare this to regions defined as noninvasive by DTI. From our knowledge of the biology of the invasive margin we would expect that multimodal imaging methods will show that these DTI-defined invasive regions will appear similar to the main tumor bulk.

Materials and Methods

Patients Recruited

Fifty patients (mean age 58.2, range 31.4–71.6 years; 33 males, 17 female) were recruited preoperatively for this prospective MRI study. All patients had imaging appearances of a GBM and histological confirmation was subsequently obtained. All patients provided signed informed consent for this study that was approved by the local Research Ethics Committee.

All patients underwent resection of these tumors using 5-ALA (5-aminolevulinic) fluorescence guidance with an aim of resecting the entire contrast-enhancing tumor as defined by the surgical RANO criteria.[26] Postoperative imaging within 72 hours of surgery showed that this was achieved in 39 patients (78%).

Imaging Studies

All patients were imaged within a week prior to surgery on a 3T Magnetom Trio MR scanner (Siemens Healthcare, Erlangen, Germany), using a standard 8-channel receive head coil and transmission on the body coil. Conventional anatomical imaging sequences, diffusion tensor imaging, DSCI, and ^{1}H MR multivoxel spectroscopic imaging (CSI) were performed on all patients. The anatomical sequences included: an axial precontrast T_1-weighted sequence (relaxation time / echo time [TR/TE]: 500/8.6 msec, number of excitations [NEX]: 1, slice thickness/interslice gap: 4/1 mm, in-plane resolution: 0.74 mm, field of view [FOV]: 24 × 24 cm, 4 min 22 sec); an axial FLAIR sequence (TR/TE/TI: 7840/95/2500 msec, NEX: 1, slice thickness/interslice gap: 4/1 mm, in-plane resolution: 0.7 mm, FOV: 22.4 × 16.8 cm, 4 min 28 sec). Diffusion tensor imaging (DTI) was performed with a single-shot SE-EPI sequence (TR/TE: 8300/98 msec, slice thickness: 2 mm, no gap, in-plane resolution: 2 mm, 12 directions, 5 b-values: 350/650/1000/1300/1600 s/mm^2, FOV: 19.2 × 19.2 cm, 9 min 26 sec). DSCI was performed (TR/TE: 1500/30 msec, slice thickness: 5 mm, in-plane resolution: 2 mm, FOV 19.2 × 19.2 cm; 90 volumes acquired, 2 min 21 sec) with 9 mL of gadobutrol (Gadovist 1.0 mmol/mL) followed by a 20-mL saline flush given via a power injector at a rate of 5 mL per second after the tenth volume. Following contrast injection a postcontrast 3D T_1-weighted inversion recovery sequence was performed (MPRAGE; TR/TE/TI: 2300/2.98/900 msec, NEX: 1, slice thickness: 1 mm, no gap, in-plane resolution: 1 mm, FOV: 25.6 × 24.1 cm, 9 min 14 sec). To plan the subsequent spectroscopy, an axial T_2-weighted acquisition was performed (TR/TE: 4840/114 msec, NEX: 1, slice thickness/interslice gap: 4/1 mm, in-plane resolution: 1 mm, FOV: 22 × 16.5 cm, 1 min 33 sec). 2D multivoxel ^{1}H MRS was performed using the semi-LASER sequence,[27] with (NEX: 3) water suppression (TR/TE: 2000/35 msec, slice thickness: 20 mm, FOV: 16 × 16 cm, 16 × 16 grid with Hamming acquisition filter, 8 min 6 sec).

Postprocessing of Imaging Data

All data processing was performed offline. The DTI data were processed using the FDT toolbox in FSL (FMRIB, Oxford, UK). For each voxel, the eigenvalues (λ_1, λ_2, λ_3) were calculated and were used to construct the p and q maps using the methodology and terminology described previously.[16]

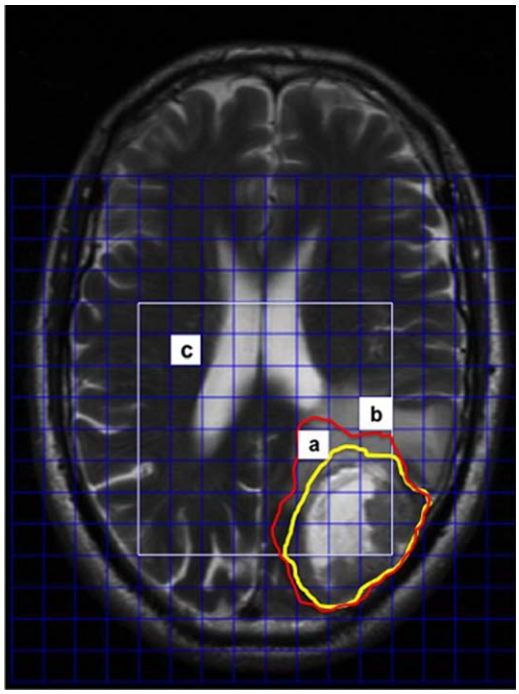

FIGURE 1: An example of the placement of ROIs. The DTI and DSCI data were coregistered to the T_2-weighted sequence used to plan the spectroscopy grid (shown in white). The *p* abnormality (red line) and *q* (yellow line) is outlined to identify the invasive margin. Regions of interest were taken from (a) the invasive region, (b) the noninvasive region, and (c) contralateral normal brain. Measures of rCBV and MRS were made from each region.

The DSCI data were processed using NordicICE (NordicNeuroLab, Bergen, Norway) and maps of rCBV were generated following contrast agent leakage correction.

The MRS data were processed using LC Model.[28] All spectra from the selected voxels were assessed visually for artifacts according to the criteria described by Kreis.[29] The values of the Cramer–Rao lower bounds indicated by the program were used to evaluate the quality and reliability of the ^{1}H spectra and values greater than 20% were discarded. The metabolites were expressed as a ratio to creatine to avoid the dilutional effects associated with varying amounts of peritumoral edema[30]

Regions of Interest (ROIs)

For each patient the contrast-enhanced T_1-weighted sequence, DTI, and DSCI parametric maps were individually coregistered to the T_2-weighted images used to plan the grid for the MRS for that patient using the FLIRT toolbox in FSL (affine transformation with 12 degrees of freedom). For the DTI images the *p* images (that had improved anatomical details) were coregistered and the transformation matrix applied to the *q* images. Coregistered images were inspected visually by S.J.P. (with 15 years neuroimaging experience) to ensure good quality of registration by outlining anatomical structures (eg, ventricles) and assessing the accuracy. The registered images were discarded and coregistration repeated if there were errors of registration greater than 2 mm. This allowed the DTI, perfusion, spectroscopy, and anatomical information to be in the same imaging space.

For each of the *p* and *q* maps, ROIs were drawn around the visible abnormality on every slice by two reviewers—a neurosurgeon with 15 years of advanced imaging experience who was involved in developing the methodology, and a radiologist with 11 years experience, using ImageJ software (National Institutes of Health, Bethesda, MD). In a random subsample of 15 patients two trained readers independently drew the ROIs twice at different timepoints to determine both the inter- and intrarater agreement.

Statistical Analysis

Three regions of interest were determined based on the spectroscopy grid, as shown in Fig. 1:

1. *Invasive:* in the DTI-defined invasive region (ie, within the area of increased *p* and outside the area of reduced *q* regions);
2. *Noninvasive:* in an area outside of the DTI-defined area (ie, outside the *p* abnormality) but in an area similar to the invasive ROI according to anatomical imaging (ie, T_2-weighted and contrast-enhanced T_1-weighted areas);
3. *Normal white matter:* in the white matter of the contralateral hemisphere, avoiding any visible pathology (as assessed by S.J.P.).

ROIs were identified where all of the MRS voxels fitted within the regions described above to avoid the issue of partial volume effects. The rCBV was calculated for each of the ROIs as a ratio to normal white matter taken from the contralateral centrum semiovale. Spectroscopic measures of N-acetylaspartate (NAA), myo-inositol (Ins), total choline (Cho) including phosphocholine and glycerylphosphorylcholine, and glutamate + glutamine (Glx) were expressed as a ratio to the total creatine (including phosphocreatine) for each ROI. We felt that it is preferable quantifying metabolites to total creatine (which varies across the tumor) to the water resonance due to problems with dilution in regions of edematous brain.[31] Similarly, the NAA/Cho ratio was determined for each ROI. All values are quoted as mean with 95% confidence interval (CI) unless otherwise stated.

Data were analyzed using IBM SPSS v. 21 (Armonk, NY) and significance was taken at the $P < 0.05$ level. Differences between the three groups were explored with analysis of variance (ANOVA), with post-hoc analysis using the Tukey-Kramer honestly significant difference (HSD) test. The receiver operator characteristic (ROC) was calculated for each of the parameters to determine which provided the best predictor of the DTI-invasive regions. This was performed by taking the values from 129 ROIs (47 invasive, 40 noninvasive, and 42 normal white matter) and used the binary classification system as invasive or not invasive (which included both the noninvasive and normal white matter ROIs) based on the DTI data. The agreement was quantified using two methods: Dice scores, which are a measure of the extent of overlap between the ROIs, and the edge Hausdorff distance[32] between the ROIs, which is a measure of the maximal distance between the edges of the ROIs being compared. As the Hausdorff distance can be sensitive to outliers, the 95th percentile of the distance was used instead. Classification of the pattern of invasion was made according to previously published criteria.[22]

Results

DTI Studies

Regions of abnormal *p* and *q* from the DTI data could be identified in all patients. Overall, 34 (68%) had a diffuse invasive pattern, 12 (24%) had a localized pattern, and 4 (8%) were minimally invasive. Thirty datasets were randomly assigned to two independent raters. There was agreement in 27 cases (90%),

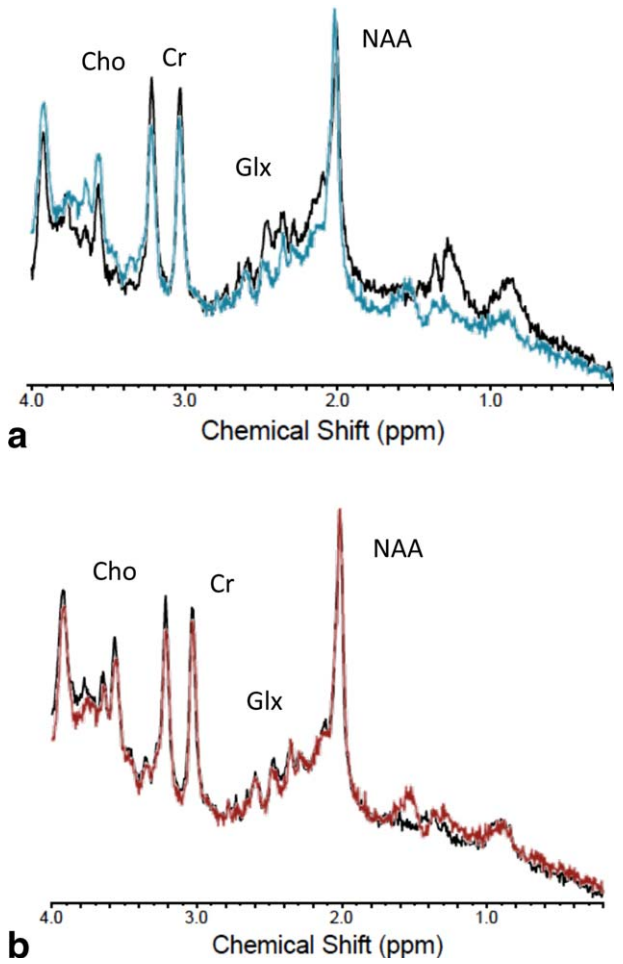

FIGURE 2: An example of MR spectra from different ROIs in a glioblastoma patient. a: The invasive region (in black) compared with the normal brain (blue). The invasive region demonstrates increased Cho and significantly reduced NAA with increased Glx. b: The noninvasive region (in black) compared with the normal brain (red). There is no significant differences between metabolites in these regions.

providing a Cohen's kappa statistic of 0.81, suggesting very good interrater agreement for the classification of the invasive phenotype. A consensus opinion was used where there was disagreement.

Interrater variability of the ROIs showed good agreement between the two raters. There was excellent agreement for the *p* regions, with mean Dice scores of 0.86 (SD 0.11) and the mean 95th centile of the edge Hausdorff distance was 8.2 mm (SD 4.7 mm). The *q* region agreement between the two raters was also good, but was not as robust as the *p* region (mean Dice scores 0.76, SD 0.16; mean 95th centile of the edge Hausdorff distance 15.7 mm, SD 9.9 mm). There was excellent intrarater agreement for both *p* (mean Dice scores 0.88, SD 0.09; mean 95th centile of the edge Hausdorff distance 7.0 mm, SD 4.9 mm) and *q* ROIs (mean Dice scores 0.85, SD 0.1; mean 95th centile of the edge Hausdorff distance 8.6 mm, SD 7.3 mm).

Perfusion Imaging

Values of rCBV could be calculated in all 50 patients. The rCBV was increased in invasive regions (mean 1.64, 95% CI 1.5–1.78; $P < 0.001$) compared to the noninvasive regions (1.14; 95% CI 1.09–1.18) and normal white matter (1.06, 95% CI 1.02–1.10; $P < 0.001$). There was no difference between rCBV values in the noninvasive and normal white matter regions ($P = 0.36$).

MRS

An example of the MR spectra in the ROIs is shown in Fig. 2. The results for the spectroscopy data are summarized in Fig. 3. Useable spectroscopic data were obtained in 41 patients (82%), dropping to 35 patients (70%) for Glx.

The NAA/Cr was significantly reduced in invasive regions (0.95, 95% CI 0.85–1.05) compared to either noninvasive (1.19, 95% CI 1.06–1.31; $P = 0.008$) or normal white matter (1.26, 95% CI 1.15–1.36; $P < 0.001$). There was no difference between noninvasive and normal white matter ($P = 1.0$).

The total choline/creatine (Cho/Cr) ratio was significantly increased in the invasive area (0.42, 95% CI 0.38–0.46) compared to both the noninvasive region (0.35, 95% CI 0.31–0.38; $P = 0.02$) and normal white matter (0.35, 95% CI 0.31–0.39; $P = 0.019$). There was no difference between these two regions ($P = 1.0$).

The glutamate + glutamine to creatine ratio (Glx/Cr) was significantly increased in the invasive region (1.54, 95% CI 1.27–1.82) compared to both the noninvasive region (1.3, 95% CI 1.13–1.47; P 0.028) and to normal white matter (1.15, 95% CI 0.99–1.31; $P = 0.034$). There was no difference between the noninvasive and normal regions ($P = 0.59$).

The choline/NAA ratio, a marker of cellular proliferation,[33] was increased in the invasive region (0.54, 95% CI 0.41–0.68) compared to both the noninvasive region (0.37, 95% CI 0.29–0.45; $P = 0.032$) and the normal white matter (0.32, 95% CI 0.25–0.39; $P = 0.004$). The latter two groups did not differ ($P = 0.78$)

The myoinositol/creatine (mI/Cr) ratio was not significantly different in either the invasive (1.2, 95% CI 0.99–1.41; $P = 0.35$) or the noninvasive regions (1.3, 95% CI 1.14–1.46; $P = 0.68$) compared to the normal white matter (1.37, 95% CI 1.24–1.5).

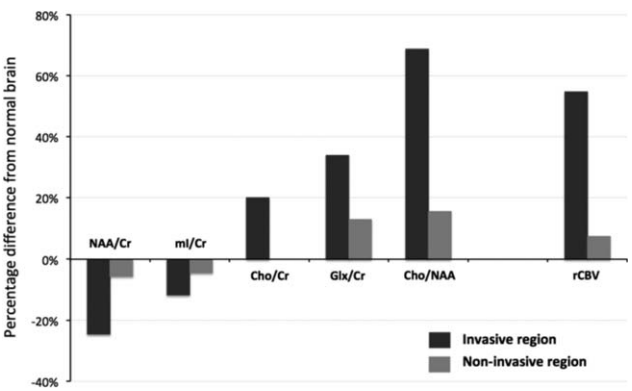

FIGURE 3: Percentage change from normal white matter.

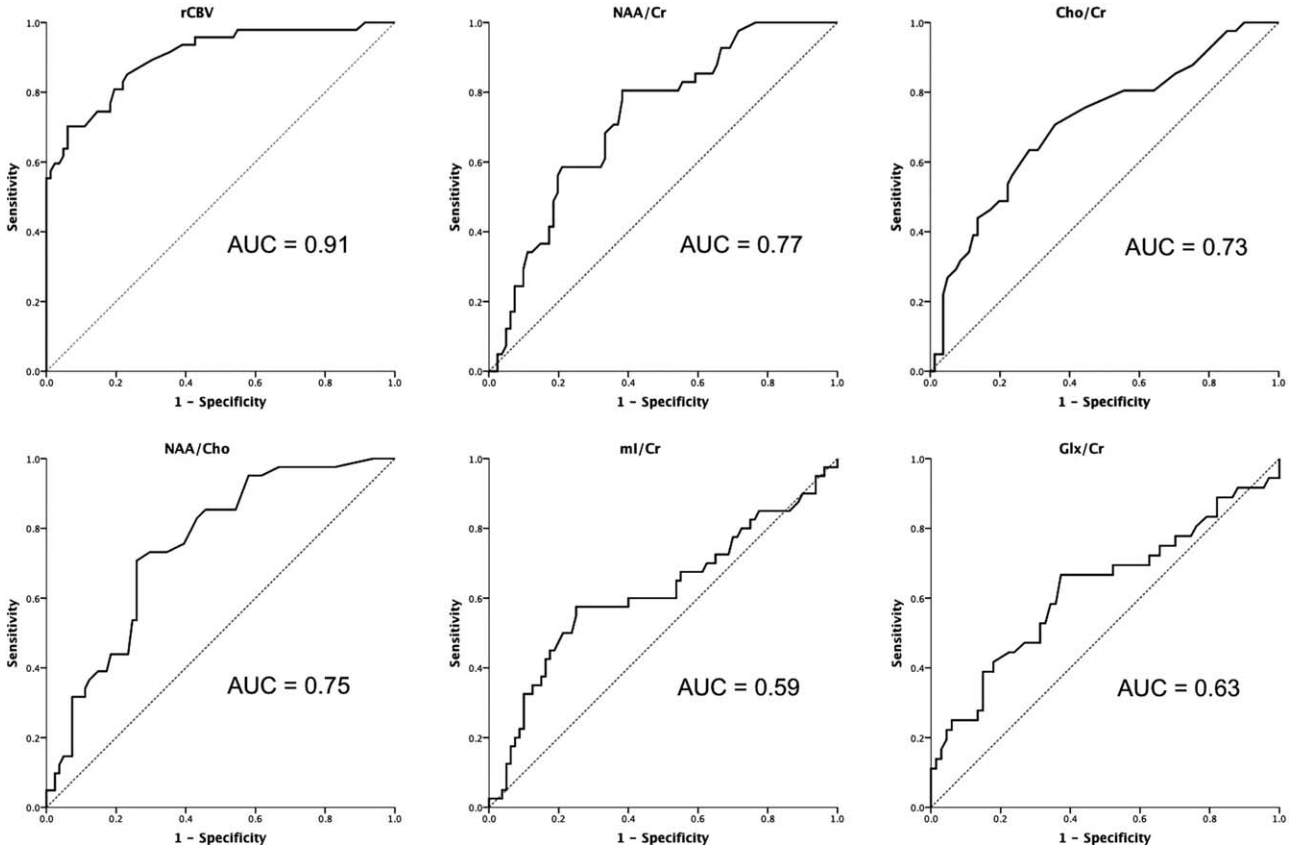

FIGURE 4: The ROC curves for the imaging parameters performance at differentiating invasive region vs. noninvasive (which includes both the noninvasive and normal ROIs). The curve for rCBV suggests that this may be the best discriminator.

Predicting Invasive Regions

The ROC showed that the rCBV data provided a better predictor of the DTI-defined invasive regions than the spectroscopic measures (data shown in Fig. 4). Using a cutoff for the rCBV of 1.25 provides a predictor with a sensitivity and specificity of 82% for identifying invasive tumor.

Discussion

Attempts to study the peritumoral region of GBMs, usually defined as the peripheral nonenhancing or edematous region, have shown that there is an increase in total choline and the Cho/NAA ratio with a reduction in total NAA.[31,34–38] Histological studies suggest that total choline and Cho/NAA increase with the degree of invasion of surrounding brain.[36] These changes are not seen in the peritumoral region of noninvasive meningiomas and metastases.[31] Similarly, areas of increased perfusion have been found in the peritumoral region of GBMs.[39–41] In this study we were able to improve the characterization of the peritumoral region using DTI, and have shown that the DTI-defined invasive region has a different local environment compared to either noninvasive or normal contralateral brain using multimodal MRI. Outlining these invasive regions showed high interrater agreement, suggesting a robust methodology. There was an increase in rCBV, Cho/Cr, Cho/NAA, and Glx/Cr, with a decrease in NAA/Cr in the invasive regions. The noninvasive regions, although showing similar appearances on conventional imaging to the invasive regions, had a similar local environment to the normal-appearing brain from the contralateral hemisphere on multimodal MRI.

In this study we defined the invasive region of the brain based purely on the DTI. Previous studies have justified this and shown that image-guided biopsies of the DTI-defined invasive region can indeed identify invasive tumor with a high degree of accuracy.[8,19] A number of studies have now shown that these DTI-defined invasive regions also predict the site of tumor progression as defined by the site where new contrast enhancement develops.[19,21,22] Our imaging methods are only sensitive enough to detect tumor cells outside of the main contrast-enhancing tumor when they are present in large numbers. As alluded to previously, it is clear that the noninvasive region will still contain tumor cells. As virtually all tumors will recur adjacent to the resection cavity,[2–5] it has been suggested that detecting the site of likely tumor progression (ie, the area with the largest number of tumor cells outside the target of surgical resection) is more important than identifying the true extent of invasion.[5]

These findings provide information on the local environment of the invasive region that correlates with our

understanding of the multiple processes that occur during invasion. As mentioned previously, the invasive cells have a different phenotype, in that they are less proliferative than enhancing tumor. The Cho/NAA ratio has been shown in some studies to correlate well with the proliferation of tumor cells:[33,42] although Cho/NAA increased in the invasive regions in the current study, it was still much lower than in other studies that looked at the enhancing tumor.[43] Others have found choline content to correlate more closely with cell density than proliferation index.[44,45] As the cell density increases, angiogenesis is stimulated by the resultant hypoxia, resulting in increased rCBV. The increase in rCBV appears to be the best measure to identify these invasive regions and has been suggested as a marker that precedes the development of contrast-enhanced tumor.[41] The release of enzymes to degrade the extracellular matrix is accompanied by glutamate release in excitotoxic concentrations.[10,46] This is consistent with the increase in Glx/Cr in these invasive areas seen in our study and reported by other groups looking at GBMs.[47–49] The net effect of these processes is the loss of neurons (measured by decrease in NAA).

In our study we failed to identify a significant change in myoinositol in the invasive region compared to normal brain. Myoinositol is thought to be involved with astrocytic integrity and regulation of brain osmosis.[50] Astrocytic proliferation is associated with an increase in myoinositol and has been reported in the peritumoral region.[31,47] As the grade of tumor increases, however, myoinositol levels decrease, so that in GBMs they are similar to normal brain.[51,52] Our data certainly show a nonsignificant trend of reduced myoinositol in DTI-defined invasive regions where previous histological studies have shown extensive invasion with high glioma cells[8] replacing other normal cell populations (including astrocytes).

The local environment of a tumor has a major influence on how that tumor will behave and respond to therapy.[53] Most imaging studies that aim to predict prognosis or response to therapy have derived measures from the contrast-enhancing tumor alone. Recent publications suggest that studying the nonenhancing component of the tumor also provides prognostic information.[54] Advances in modern neurosurgery now mean that complete resection of the contrast-enhancing tumor is achieved more often; in our series, a complete resection of the contrast-enhancing tumor was achieved in 78% of cases. The result is that nonenhancing tumor margin will be the site of progressive tumor. Studying these regions may be more relevant to prognostication and response to therapies performed after surgical treatments.

One major limitation of our work is the difference in resolution, slice thickness, and gaps between the anatomical imaging, DTI imaging ($2 \times 2 \times 2$ mm voxel size providing whole brain coverage), DSC imaging ($2 \times 2 \times 5$ mm voxel size providing whole brain coverage), and our single-slice multivoxel spectroscopic imaging ($10 \times 10 \times 20$ mm voxel size). This will lead to issues with the coregistration and lead to partial volume errors. The difference in voxel size is particularly critical for the MRS data and means that the spectral pattern will be dependent on the relative amount of tumor to normal brain in these invasive regions. But these limitations will be the same for each of the three ROIs we compared for each patient. Our findings would suggest that in the DTI-defined invasive regions there is a high proportion of tumor cells, whereas in noninvasive regions there is more normal brain. Other groups have published their experience of 3D spectroscopy—but even then only managed a voxel size of $10 \times 10 \times 10$ mm.[55] They described changes in NAA and Cho in normal-appearing white matter surrounding gliomas. This study used a longer echo time (70 msec) and as a result was not able to analyze metabolites with smaller concentrations (eg, myoinositol and glutamate + glutamine). Newer sequences providing 3D short echo spectroscopy have been developed and shown to be reproducible[56] but still suffer from poor resolution compared to DTI and DSCI and long acquisition times that make it difficult to use for multimodal imaging in this population. It is likely, however, that these methods will be utilized in the future.

In conclusion, by using DTI to define the limits of invasion we see changes in the local environment in invasive regions that are not seen in noninvasive brain and which fit with our understanding of glioma invasion.

Acknowledgment

Contract grant sponsor: National Institutes of Health Research Clinician Scientist Fellowship.

Conflict of Interest

The authors declare no conflicts of interest.

References

1. Stummer W, Meinel T, Ewelt C, et al. Prospective cohort study of radiotherapy with concomitant and adjuvant temozolomide chemotherapy for glioblastoma patients with no or minimal residual enhancing tumor load after surgery. J Neurooncol 2012:1–9.
2. Oppitz U, Maessen D, Zunterer H, Richter S, Flentje M. 3D-recurrence-patterns of glioblastomas after CT-planned postoperative irradiation. Radiother Oncol 1999;53:53–57.
3. Lee SW, Fraass BA, Marsh LH, et al. Patterns of failure following high-dose 3-D conformal radiotherapy for high-grade astrocytomas: a quantitative dosimetric study. Int J Radiat Oncol Biol Phys 1999;43:79–88.
4. Brandes AA, Tosoni A, Franceschi E, et al. Recurrence pattern after temozolomide concomitant with and adjuvant to radiotherapy in newly diagnosed patients with glioblastoma: correlation with MGMT promoter methylation status. J Clin Oncol 2009;27:1275–1279.

5. Chang EL, Akyurek S, Avalos T, et al. Evaluation of peritumoral edema in the delineation of radiotherapy clinical target volumes for glioblastoma. Int J Radiat Oncol Biol Phys 2007;68:144–150.
6. Berens ME, Giese A. "... those left behind." Biology and oncology of invasive glioma cells. Neoplasia 1999;1:208–219.
7. Kelly PJ, Daumas-Duport C, Kispert DB, Kall BA, Scheithauer BW, Illig JJ. Imaging-based stereotaxic serial biopsies in untreated intracranial glial neoplasms. J Neurosurg 1987;66:865–874.
8. Price SJ, Jena R, Burnet NG, et al. Improved delineation of glioma margins and regions of infiltration with the use of diffusion tensor imaging: an image-guided biopsy study. Am J Neuroradiol 2006;27: 1969–1974.
9. Giese A, Loo MA, Tran N, Haskett D, Coons SW, Berens ME. Dichotomy of astrocytoma migration and proliferation. Int J Cancer 1996;67: 275–282.
10. Ye ZC, Sontheimer H. Glioma cells release excitotoxic concentrations of glutamate. Cancer Res 1999;59:4383–4391.
11. Deryugina EI, Bourdon MA, Luo GX, Reisfeld RA, Strongin A. Matrix metalloproteinase-2 activation modulates glioma cell migration. J Cell Sci 1997;110(Pt 19):2473–2482.
12. Zuniga RM, Torcuator R, Jain R, et al. Efficacy, safety and patterns of response and recurrence in patients with recurrent high-grade gliomas treated with bevacizumab plus irinotecan. J Neurooncol 2009;91:329–336.
13. Price S, Burnet N, Donovan T, et al. Diffusion tensor Imaging of brain tumours at 3 T: a potential tool for assessing white matter tract invasion? Clin Radiol 2003;58:455–462.
14. Wang S, Kim SJ, Poptani H, et al. Diagnostic utility of diffusion tensor imaging in differentiating glioblastomas from brain metastases. AJNR Am J Neuroradiol 2014;35:928–934.
15. Provenzale JM, McGraw P, Mhatre P, Guo AC, Delong D. Peritumoral brain regions in gliomas and meningiomas: investigation with isotropic diffusion-weighted MR imaging and diffusion-tensor MR imaging. Radiology 2004;232:451–460.
16. Pena A, Green H, Carpenter T, Price S, Pickard J, Gillard J. Enhanced visualization and quantification of magnetic resonance diffusion tensor imaging using the p : q tensor decomposition. Br J Radiol 2006;79: 101–109.
17. Price S, Pena A, Burnet N, et al. Tissue signature characterisation of diffusion tensor abnormalities in cerebral gliomas. Eur Radiol 2004;14: 1909–1917.
18. Wang W, Steward CE, Desmond PM. Diffusion tensor imaging in glioblastoma multiforme and brain metastases: the role of p, q, L, and fractional anisotropy. AJNR Am J Neuroradiol 2009;30:203–208.
19. Castellano A, Donativi M, Bello L, et al. Evaluation of changes in gliomas structural features after chemotherapy using DTI-based functional diffusion maps (fDMs): a preliminary study with intraoperative correlation. In: Proc 19th Annual Meeting ISMRM, Montreal; 2011. p 2411.
20. Mohsen LA, Shi V, Jena R, Gillard JH, Price SJ. Diffusion tensor invasive phenotypes can predict progression-free survival in glioblastomas. Br J Neurosurg 2013;27:419–424.
21. Price S, Pena A, Burnet N, Pickard J, Gillard J. Detecting glioma invasion of the corpus callosum using diffusion tensor imaging. Br J Neurosurg 2004;18:391–395.
22. Price S, Jena R, Burnet N, Carpenter T, Pickard J, Gillard J. Predicting patterns of glioma recurrence using diffusion tensor imaging. Eur Radiol 2007;17:1675–1684.
23. Sugahara T, Korogi Y, Kochi M, et al. Correlation of MR imaging-determined cerebral blood volume maps with histologic and angiographic determination of vascularity of gliomas. AJR Am J Roentgenol 1998;171:1479–1486.
24. Aronen HJ, Pardo FS, Kennedy DN, et al. High microvascular blood volume is associated with high glucose uptake and tumor angiogenesis in human gliomas. Clin Cancer Res 2000;6:2189–2200.
25. Price SJ, Green HA, Dean AF, Joseph J, Hutchinson PJ, Gillard JH. Correlation of MR relative cerebral blood volume measurements with cellular density and proliferation in high-grade gliomas: an image-guided biopsy study. AJNR Am J Neuroradiol 2011;32:501–506.
26. Vogelbaum MA, Jost S, Aghi MK, et al. Application of novel response/progression measures for surgically delivered therapies for gliomas. Neurosurgery 2012;70:234–244.
27. Scheenen TW, Klomp DW, Wijnen JP, Heerschap A. Short echo time 1H-MRSI of the human brain at 3T with minimal chemical shift displacement errors using adiabatic refocusing pulses. Magn Reson Med 2008;59:1–6.
28. Provencher SW. Estimation of metabolite concentrations from localized in vivo proton NMR spectra. Magn Reson Med 1993;30: 672–679.
29. Kreis R. Issues of spectral quality in clinical 1H-magnetic resonance spectroscopy and a gallery of artifacts. NMR Biomed 2004;17:361–381.
30. Kamada K, Houkin K, Hida K, et al. Localized proton spectroscopy of focal brain pathology in humans: significant effects of edema on spin-spin relaxation time. Magn Reson Med 1994;31:537–540.
31. Wijnen JP, Idema AJ, Stawicki M, et al. Quantitative short echo time 1H MRSI of the peripheral edematous region of human brain tumors in the differentiation between glioblastoma, metastasis, and meningioma. J Magn Reson Imaging JMRI 2012;36:1072–1082.
32. Mostayed A, Garlapati RR, Joldes GR, et al. Biomechanical model as a registration tool for image-guided neurosurgery: evaluation against BSpline registration. Ann Biomed Eng 2013;41:2409–2425.
33. McKnight TR, Lamborn KR, Love TD, et al. Correlation of magnetic resonance spectroscopic and growth characteristics within Grades II and III gliomas. J Neurosurg 2007;106:660–666.
34. Sijens PE, Oudkerk M. 1H chemical shift imaging characterization of human brain tumor and edema. Eur Radiol 2002;12:2056–2061.
35. Di Costanzo A, Scarabino T, Trojsi F, et al. Multiparametric 3T MR approach to the assessment of cerebral gliomas: tumor extent and malignancy. Neuroradiology 2006;48:622–631.
36. Croteau D, Scarpace L, Hearshen D, et al. Correlation between magnetic resonance spectroscopy imaging and image-guided biopsies: semiquantitative and qualitative histopathological analyses of patients with untreated glioma. Neurosurgery 2001;49: 823–829.
37. Pirzkall A, Li X, Oh J, et al. 3D MRSI for resected high-grade gliomas before RT: tumor extent according to metabolic activity in relation to MRI. Int J Radiat Oncol Biol Phys 2004;59:126–137.
38. Bieza A, Krumina G. Magnetic resonance study on fractional anisotropy and neuronal metabolite ratios in peritumoral area of cerebral gliomas. Medicina 2012;48:497–506.
39. Price SJ, Green HAL, Dean AF, Joseph J, Hutchinson PJ, Gillard JH. Correlation of MR relative cerebral blood volume measurements with cellular density and proliferation in high-grade gliomas: an image-guided biopsy study. Am J Neuroradiol 2011;32:501–506.
40. Lehmann P, Vallee JN, Saliou G, et al. Dynamic contrast-enhanced T2*-weighted MR imaging: a peritumoral brain oedema study. J Neuroradiol 2009;36:88–92.
41. Blasel S, Franz K, Ackermann H, Weidauer S, Zanella F, Hattingen E. Stripe-like increase of rCBV beyond the visible border of glioblastomas: site of tumor infiltration growing after neurosurgery. J Neurooncol 2011;103:575–584.
42. Guo J, Yao C, Chen H, et al. The relationship between Cho/NAA and glioma metabolism: implementation for margin delineation of cerebral gliomas. Acta Neurochir (Wien) 2012;154:1361–1370; discussion 1370.
43. Laprie A, Catalaa I, Cassol E, et al. Proton magnetic resonance spectroscopic imaging in newly diagnosed glioblastoma: predictive value for the site of postradiotherapy relapse in a prospective longitudinal study. Int J Radiat Oncol Biol Phys 2008;70:773–781.

44. Gupta RK, Cloughesy TF, Sinha U, et al. Relationships between choline magnetic resonance spectroscopy, apparent diffusion coefficient and quantitative histopathology in human glioma. J Neurooncol 2000;50:215–226.

45. Nafe R, Herminghaus S, Raab P, et al. Preoperative proton-MR spectroscopy of gliomas—correlation with quantitative nuclear morphology in surgical specimen. J Neurooncol 2003;63:233–245.

46. Marcus HJ, Carpenter KL, Price SJ, Hutchinson PJ. In vivo assessment of high-grade glioma biochemistry using microdialysis: a study of energy-related molecules, growth factors and cytokines. J Neurooncol 2010;97:11–23.

47. Kallenberg K, Bock HC, Helms G, et al. Untreated glioblastoma multiforme: increased myo-inositol and glutamine levels in the contralateral cerebral hemisphere at proton MR spectroscopy. Radiology 2009;253: 805–812.

48. Chawla S, Zhang Y, Wang S, et al. Proton magnetic resonance spectroscopy in differentiating glioblastomas from primary cerebral lymphomas and brain metastases. J Comput Assist Tomogr 2010;34:836–841.

49. Ramadan S, Andronesi OC, Stanwell P, Lin AP, Sorensen AG, Mountford CE. Use of in vivo two-dimensional MR spectroscopy to compare the biochemistry of the human brain to that of glioblastoma. Radiology 2011;259:540–549.

50. Brand A, Richter-Landsberg C, Leibfritz D. Multinuclear NMR studies on the energy metabolism of glial and neuronal cells. Dev Neurosci 1993;15:289–298.

51. Castillo M, Smith JK, Kwock L. Correlation of myo-inositol levels and grading of cerebral astrocytomas. AJNR Am J Neuroradiol 2000;21: 1645–1649.

52. Candiota AP, Majos C, Julia-Sape M, et al. Non-invasive grading of astrocytic tumours from the relative contents of myo-inositol and glycine measured by in vivo MRS. JBR-BTR 2011;94:319–329.

53. Persano L, Rampazzo E, Basso G, Viola G. Glioblastoma cancer stem cells: role of the microenvironment and therapeutic targeting. Biochem Pharmacol 2013;85:612–622.

54. Jain R, Polsson LM, Gutman D, et al. Outcome prediction in patients with glioblastoma by using imaging, clinical, and genomic biomarkers: focus on the nonenhancing component of the tumor. Radiology 2014; 272:484–493.

55. Maudsley AA, Roy B, Gupta RK, et al. Association of metabolite concentrations and water diffusivity in normal appearing brain tissue with glioma grade. J Neuroimaging 2014;24:585–589.

56. Ding XQ, Maudsley AA, Sabati M, Sheriff S, Dellani PR, Lanfermann H. Reproducibility and reliability of short-TE whole-brain MR spectroscopic imaging of human brain at 3T. Magn Reson Med 2015;73:521–528.

Author/s:
Price, SJ; Young, AMH; Scotton, WJ; Ching, J; Mohsen, LA; Boonzaier, NR; Lupson, VC; Griffiths, JR; McLean, MA; Larkin, TJ

Title:
Multimodal MRI can identify perfusion and metabolic changes in the invasive margin of glioblastomas.

Date:
2016-02

Citation:
Price, S. J., Young, A. M. H., Scotton, W. J., Ching, J., Mohsen, L. A., Boonzaier, N. R., Lupson, V. C., Griffiths, J. R., McLean, M. A. & Larkin, T. J. (2016). Multimodal MRI can identify perfusion and metabolic changes in the invasive margin of glioblastomas.. J Magn Reson Imaging, 43 (2), pp.487-494. https://doi.org/10.1002/jmri.24996.

Persistent Link:
http://hdl.handle.net/11343/272375

File Description:
Published version